Si L- and K-edge x-ray-absorption near-edge spectroscopy of gas-phase $Si(CH_3)_x(OCH_3)_{4-x}$: Models for solid-state analogs

D. G. J. Sutherland, M. Kasrai, G. M. Bancroft,* Z. F. Liu, and K. H. Tan
Department of Chemistry and Canadian Institute for Synchrotron Radiation, University of Western Ontario, London, Ontario, Canada N6A 5B7
and Canadian Synchrotron Radiation Facility, Synchrotron Radiation Center, University of Wisconsin, Stoughton, Wisconsin 53589
(Received 3 May 1993)

Both the L- and K-edge x-ray-absorption near-edge spectra for the five compounds $Si(OCH_3)_x(CH_3)_{4-x}$ ($x=0$ to 4) are reported. The spectra of the two end members of the series, $Si(OCH_3)_4$ and $Si(CH_3)_4$, are compared to the spectra of their respective solid-state analogs, SiO_2 and SiC. The L-edge spectra of gaseous $Si(OCH_3)_4$ and solid SiO_2 are qualitatively identical; while the L-edge spectra of gaseous $Si(CH_3)_4$ and its solid-state counterpart, SiC, show strong similarities. MS-$X\alpha$ calculations were performed for the two species $Si(OCH_3)_4$ and $Si(CH_3)_4$ for the Si $2p$, $2s$, and $1s$ regions and used to assign the spectra for both compounds. By comparison of molecular-orbital diagrams of $Si(OCH_3)_4$ and SiO_2, the first two transitions in the L-edge spectra of SiO_2 have been assigned to transitions from the Si $2p$ to orbitals of a_1^* and t_2^* symmetry. In addition to SiO_2, the L-edge spectra of the isoelectronic species PO_4^{3-}, SO_4^{2-}, and ClO_4^- are also assigned in a similar manner. Compared to the L edge, the K-edge region of the gas-phase compounds is found to have less in common with the spectra of the solid-state analogs. In the K-edge region, peaks from the extended band structure and/or multiple scattering are evident in the solid-state compounds. These peaks are not present, as expected, in the gas-phase models or in the theoretical calculations on the gas-phase compounds. These multiple-scattering peaks are not seen in the L-edge solid-state spectra because of the strong shape resonances peaks in this region.

INTRODUCTION

Largely due to its importance in the semiconductor industry, the Si L edge and valence-band spectra of SiO_2 have been a topic of continued interest throughout the past 25 years.[1–9] The tetrahedral symmetry of SiO_2 enables a molecular-orbital interpretation of the electronic structure[1] and most of the theoretical work has centered on the SiO_4^{4-} ion.[10,11] This ion, however, is not a particularly good model for SiO_2 for two reasons.[10] First, it is an ion with a large negative charge, and second, unlike SiO_2, where each O is bonded to two Si's, the oxygen atoms in SiO_4^{4-} each have a single dangling bond.

Surprisingly, very little work has been done to compare gas-phase analogs and solid-state spectra. Dehmer[1] has compared the Si $2p$ x-ray-absorption near-edge spectra (XANES) of gaseous $SiCl_4$ and SiF_4 to that of solid-state SiO_2 and SiF_6^{2-} to demonstrate the similarities between the tetrahedral and octahedral symmetries. In doing so, he showed that the spectra of the gas-phase compounds and the solid-state SiO_2 are qualitatively similar. Furthermore, he was able to delineate the correspondence between the energies of the molecular orbitals of Si compounds with different symmetries (octahedral versus tetrahedral). More recently Filatova, Vinogrdov, and Zimkina[7] have published a similar comparison of the L-edge spectrum of SiO_2 and the solid-state spectra of SiF_4 and SiH_4.

For reasons unknown, no investigation has been made of the more obvious analog, tetramethoxy silane, $Si(OCH_3)_4$. The tetrahedral arrangement of four oxygens around the silicon atom is identical to that in the SiO_2 structure, and the four methyl groups simulate the environment of a second Si bonded to each O. For these reasons it is felt that this is a far superior experimental model than $SiCl_4$, SiF_4, or SiH_4, and possibly a better theoretical model than SiO_4^{4-}.

In this paper we present the following. First, a complete analysis of the high-resolution XANES spectra of the Si $1s$, $2s$, and $2p$ edges of the five compounds in the series $Si(CH_3)_x(OCH_3)_{4-x}$; second, the theoretical cross-section calculations of the two end members of the series, tetramethyl silane [TMS, $Si(CH_3)_4$] and tetramethoxy silane [TMOS, $Si(OCH_3)_4$]; and third, a comparison of the gas-phase spectra with existing spectra of solid-state analogs (i.e., silicon carbide and silicon dioxide). The objectives of this paper are threefold. First, to show that the gas-phase XANES spectra of $Si(OCH_3)_4$ and $Si(CH_3)_4$ are indeed excellent analogs for the Si $2p$ spectra of the solid-state compounds SiO_2 and SiC, respectively. The second objective is to show that the MS-$X\alpha$ cross-section calculations of the molecular spectra can readily explain both the gas-phase *and* the solid-state spectra. The third and final objective of this paper is to show that the L-edge spectra of the compounds MO_4 (M =Si,P,S,Cl) are all qualitatively similar and can be explained analogously.

EXPERIMENTAL AND THEORETICAL

All samples were purchased commercially from Huls America with purity greater than 99% and used without

 ©1993 The American Physical Society

further purification. The photoabsorption spectra of the Si 2*s* and 2*p* edges of all five compounds were recorded in the gas phase with a path length of 30 cm and a gas pressure of 30 m torr. The attenuation of the radiation by the sample was measured by monitoring the electrical current from a gold diode placed at the end of the gas cell.

All *L*-edge spectra were recorded using the CSRF Mark IV Grasshopper monochromator[12] at the Aladdin synchrotron of the University of Wisconsin at Madison. The monochromator employs an 1800 groove/mm grating which yields a minimum practical photon resolution of 0.05 eV at 105-eV photon energy. The accuracy of the monochromator was calibrated by recording the position of the Kr $3d_{5/2}$ edge which has a binding energy of 93.798 eV.[13] The peak positions of the spectra in this paper are accurate to within ±0.05 eV.

The five spectra of the Si 1*s* region were recorded in the gas phase with a path length of 50 cm using a single ionization chamber on the CSRF double crystal[14] beamline at the Aladdin Synchrotron at the University of Wisconsin. The double crystal monochromator (DCM) employs twin InSb crystals and has a resolution of better than 0.80 eV at the Si 1*s* edge (approximately 1840 eV). Calibration of the monochromator was done by recording the Si 1*s* spectrum of $SiCl_4$ and comparing this to previously published work.[15,16] Peak positions are accurate to within ±0.1 eV. The photoelectron spectrometer used to record the valence-band spectrum of $Si(OCH_3)_4$ has been described in detail elsewhere.[17]

The *L*-edge solid-state XANES spectrum of SiO_2 was recorded on the CSRF grasshopper beamline and the *K*-edge spectrum was recorded on the CSRF DCM beamline. The spectra of other solid-state compounds [$(Ca)_3(PO_4)_2$, Na_2SO_4, and $NaClO_4$] were all recorded on the CSRF grasshopper beamline. All solid-state spectra were recorded in the total electron yield mode.[18]

Theoretical results, oscillator strengths, and continuum cross sections of the Si 1*s*, 2*s*, and 2*p* edges for the two molecules TMS [$Si(CH_3)_4$] and TMOS [$Si(OCH_3)_4$] were carried out using the MS-$X\alpha$ method[19] and the continuum cross-section program of Davenport.[20] The true symmetry of TMOS is S_4 which is not amenable to the MS-$X\alpha$ technique and so the calculations on this molecule were carried out in C_{2v} symmetry. The calculations for TMS were carried out in the true tetrahedral symmetry. In both cases a latter tail[21] was added to account for the potential's asymptotic behavior at large distances.

Structural data for these two molecules were obtained from gas-phase electron-diffraction studies,[22] and were used to calculate the atomic positions for the calculations. The values used for the sphere size, atomic exchange parameters, and l_{max} values for all regions are listed in Table I. The cross-section and oscillator-strength calculations for all edges were carried out using a converged transition-state potential created by removing half an electron from the appropriate core level in the ground state. All processes allowed by the dipole selection rules were included in the bound state and continuum cross-section calculations.

RESULTS AND DISCUSSION

The Si 2*p* edge

Figure 1 shows the Si 2*p* and 2*s* XANES photoabsorption spectra of the five compounds in the series $Si(CH_3)_x(OCH_3)_{4-x}$ from 90 to 190 eV. All five spectra are superimposed upon the background of a decreasing valence cross section. Because the decrease in the valence cross section is much greater for O in this region than it is for C, the effect of the background becomes less prominent as the number of methoxy groups in the molecule decreases.

The overall shapes of the five spectra in Fig. 1 are very similar to each other and to the spectra of other silicon-

TABLE I. The sphere radii, α values, and initial- and final-state values of l_{max} for the calculations of the two molecules $Si(OCH_3)_4$ and $Si(CH_3)_4$.

Molecule	Region	Radius (a.u.)	α	l_{max} Initial	l_{max} Final
$Si(OCH_3)_4$	Outer Sphere	6.42	0.7545	4	7
	Si	1.99	0.7275	3	5
	O_1	1.43	0.7445	2	4
	O_2	1.43	0.7445	2	4
	C_1	1.51	0.7593	2	4
	C_2	1.51	0.7593	2	4
	H_1	1.04	0.7772	0	2
	H_2	1.04	0.7772	0	2
	H_3	1.01	0.7772	0	2
	H_4	1.01	0.7772	0	2
$Si(CH_3)_4$	Outer Sphere	5.70	0.7620	4	6
	Si	2.06	0.7275	3	5
	C	1.48	0.7593	2	4
	H	1.00	0.7772	0	2

containing[1,23,24] molecules such as $SiCl_4$ and SiF_4. The peaks at ~114 and ~128 eV are labeled G and H, respectively (labels A to F are reserved for the preedge features in Fig. 2) and are present in all five spectra with peak H shifting slightly to lower energy as the more electronegative methoxy groups are replaced with methyl groups (see Table II). Features resulting from transitions of the Si 2s electrons at ~155 eV are not labeled in Fig. 1 but will be discussed separately in reference to the K-edge spectra (see Figs. 8–11).

For the sake of consistency, throughout this paper, wherever possible, peaks that arise from transitions to the same orbitals will be labeled with the same letter. In the case of L-edge spectra, the $p_{3/2}$ and $p_{1/2}$ components of the transition will be labeled with a letter and its *prime* (i.e., peaks A and A'). Figure 2 shows the preedge region of the same five compounds shown in Fig. 1 on an expanded scale from 101 to 111 eV, and the positions of the peaks from Fig. 2 (peaks A to F) and the peaks from Fig. 1 (peaks G and H) are listed in Table II. The position of the flag that marks the Si $2p_{3/2}$ adiabatic ionization potential is taken from Ref. 25.

Immediately obvious is the increase in complexity of the spectra as you move through the series from TMOS [$Si(OCH_3)_4$] to TMS [$Si(CH_3)_4$]. Nine peaks are observed in Fig. 2 for the preedge region of TMS (some of which result from multiple transitions), in accord with previous work on this molecule,[23] while only four peaks are observed for TMOS. The TMS peaks have been assigned to Si 2p to Rydberg transitions.[23] In contrast, the TMOS spectrum is more similar to that of SiF_4,[23] in which the major peaks are due to Si 2p to antibonding transitions. In terms of Dehmer's *effective potential barrier model*[1] this decrease in complexity from TMS to TMOS is due to the creation of a potential barrier by the electronegative oxygen atoms allowing transitions only to an inner and outer potential well and thereby obscuring the Rydberg fine structure in those compounds as the number of methoxy groups increases. By the time two methoxy groups have been replaced with methyl groups the preedge region (Fig. 2) has become more like the spectrum of TMS while the post-edge region (Figs. 1 and 2) has remained similar to that of TMOS.

Figure 3(a) shows the spectra of TMOS and SiO_2 and a density of states (DOS) calculation for SiO_2 (digitized from Ref. 26) all plotted on the same axes while Fig. 3(b) shows the spectrum of TMS and Filatova's spectrum of silicon carbide (digitized from Ref. 7). The peak positions for the spectrum of SiO_2 and the DOS calculations in Fig. 3(a) are detailed in the last two columns of Table II. The spectra of SiO_2 and TMOS are remarkably similar; each has a sharp doublet centered at ~105.5 eV [peaks A and A' in Fig. 3(a)] followed by a broader peak at ~107.5 eV (peak C). Peak D is a distinct feature in the solid-state spectrum but shows up only as a shoulder on peak C in the gas-phase analog. This is followed by a broad, asymmetric peak at ~114 eV and a very broad peak at ~130 eV (peaks G and H, respectively). The initial doublet is shifted to higher energy in the spectrum of SiO_2; however, all other peaks occur at almost exactly the

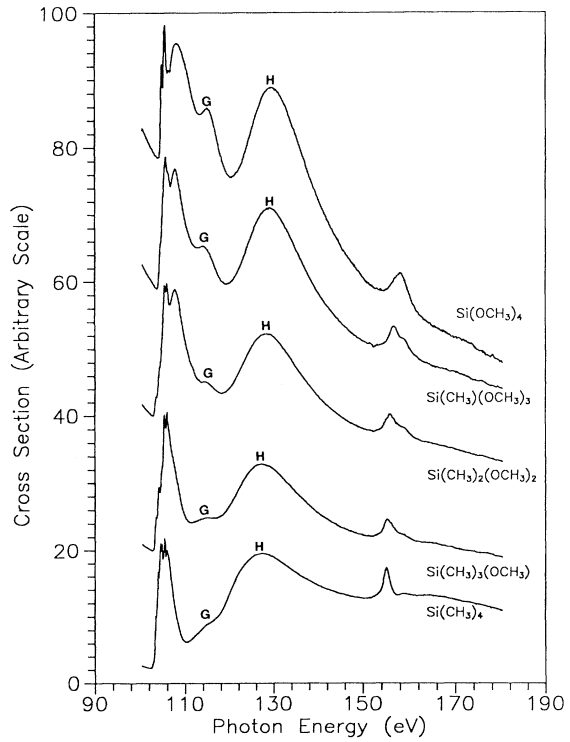

FIG. 1. The Si 2p and 2s XANES spectra of $Si(OCH_3)_x(CH_3)_{4-x}$ (x =0 to 4).

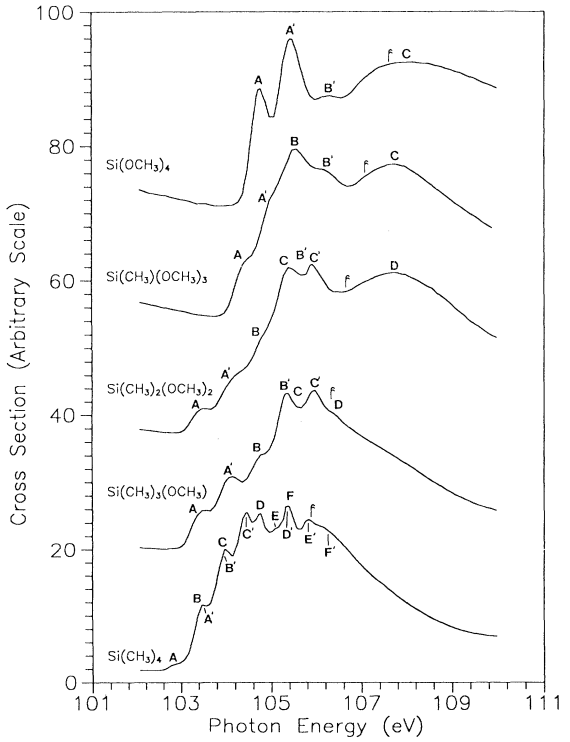

FIG. 2. The Si 2p XANES spectra of $Si(OCH_3)_x(CH_3)_{4-x}$ (x =0 to 4).

TABLE II. The peak positions (in eV ± 0.05 eV) of the spectra shown in Figs. 1, 2, and 3(a), and the position of the Si $2p_{3/2}$ and $2p_{1/2}$ adiabatic binding energies from Ref. 24. Si 2p ionization energies for SiO_2 were taken from Ref. 37.

	Molecule $Si(OCH_3)_x(CH_3)_{4-x}$			(Figs. 1 and 2)		Fig. 3(a)	
Peak	$x=0$	$x=1$	$x=2$	$x=3$	$x=4$	SiO_2	DOS (+ 95.9 eV)
A	102.82	103.52	103.52	104.47	104.76	105.57	105.9
A'	103.48	104.12	104.15	105.05	105.42	106.10	
B	103.38	104.78	104.84	105.52			
B'	103.98	105.34	105.52	106.13	106.27		
C	104.00	105.39	105.40	107.69	108.10	108.04	107.9
C'	105.15	105.95	105.98				
D	104.74	106.38	107.71		111.31	111.39	111.1
D'	105.37						
E	105.15						
E'	105.83						
F	105.37						
F'	106.26						
G	114.65	114.55	114.02	114.19	114.82	114.51	118.1
H	126.85	127.10	128.18	128.70	129.36	130.53	
Si $2p_{3/2}$	105.86	106.3(1)	106.6(1)	107.0(1)	107.42	103.8(1)*	
Si $2p_{1/2}$	106.47	106.9(1)	107.2(1)	107.6(1)	108.03	104.4(1)*	

same position and have similar intensity.

The conduction band in the DOS calculation has been shifted by 95.9 eV to align it with the *L*-edge XANES spectrum of SiO_2. It is interesting to note that although the DOS calculations shows only the relative position of the unoccupied states (and not the *s* or *p* character of these states or the transition probabilities to these states) the overall shape of the DOS plot is quite similar to that of the Si 2p spectrum of SiO_2. Peaks *A*, *C*, and *D* have similar relative positions in the DOS calculation and the SiO_2 spectrum. The difference in relative intensity could well be due to the different *s* and *p* character of the conduction-band data. Obviously peak *G* is not well reproduced by the DOS calculations. Unfortunately, the original authors[26] did not assign or even discuss the *s* and *p* character of the conduction band and, as such, no direct comparison can be made with the current calculations (see Figs. 4 and 5). A more detailed comparison of the DOS calculation[26] and the SiO_2 spectrum will be dealt with in a future publication.[27] In Fig. 3(b) the fine structure in the preedge region of the SiC spectrum is washed out compared to the spectrum of TMS but the spectra are otherwise qualitatively similar. Better quality spectra of SiC are required for a more detailed comparison.

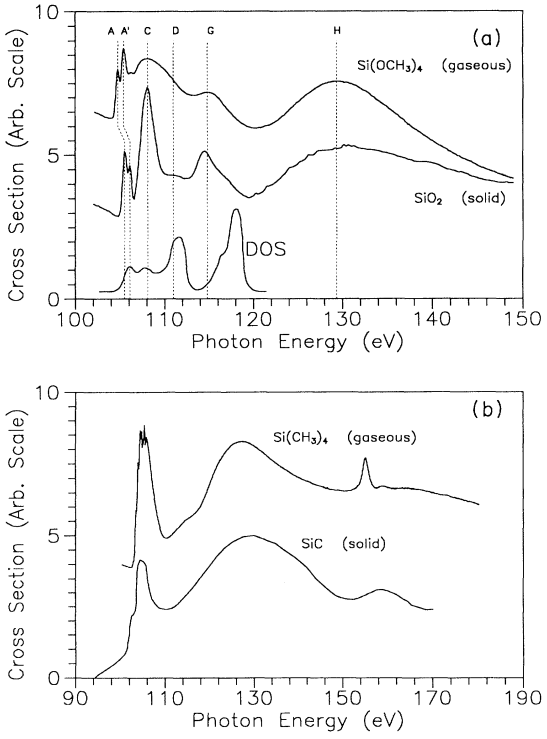

FIG. 3. (a) The Si 2p gas-phase spectra $Si(OCH_3)_4$ (top), solid state SiO_2 (middle), and DOS calculation (bottom). (b) The Si 2p gas-phase spectra of $Si(CH_3)_4$ (top) and solid state SiC (bottom).

Despite the similar general appearance, there are, however, some differences between the spectrum of the solid-state SiO_2 and the gas-phase TMOS: the relative intensities of the initial doublet are reversed in the gas and solid state, and the small peak labeled *B'* in the spectrum of TMOS (Fig. 2) is not present in the spectrum of SiO_2. Both of these differences can be rationalized by analysis of the MS-$X\alpha$ simulation which is discussed below. Peak *C*, centered at ~107 eV, is much sharper in the solid-state spectrum than it is in the gas phase and this may be the result of splitting of the energy levels due to the lower symmetry of TMOS compared with the tetrahedral symmetry of SiO_2. Also, there is a small feature in the spectrum of SiO_2 at ~111 eV [peak *D*, Fig. 3(a)] that is washed out by peak *C* in the spectrum of TMOS and, peak *G* has a slight shoulder on the high-energy side in the solid state that is not present in the gas phase. The

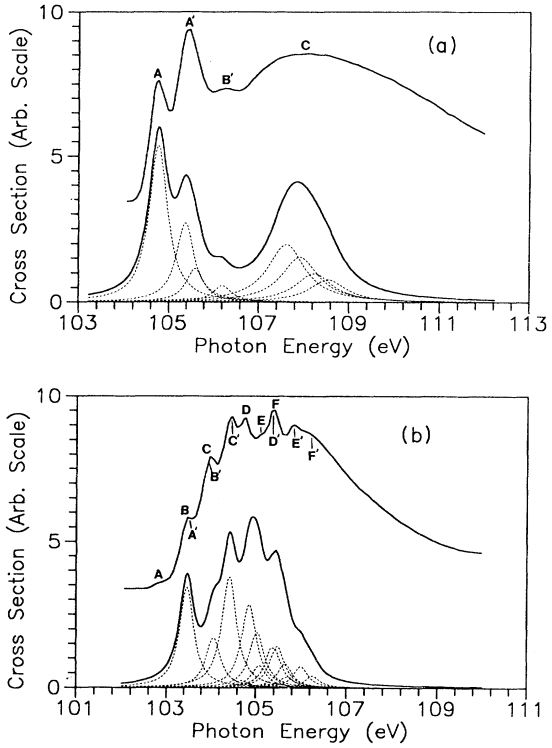

FIG. 4. (a) The Si $2p$ preedge XANES spectra of $Si(OCH_3)_4$ (top) and the corresponding MS-$X\alpha$ SCF simulation (bottom). (b) The Si $2p$ preedge XANES spectra of $Si(CH_3)_4$ (top) and the corresponding MS-$X\alpha$ SCF simulation (bottom). Dashed lines in both (a) and (b) mark the positions of the individual transitions.

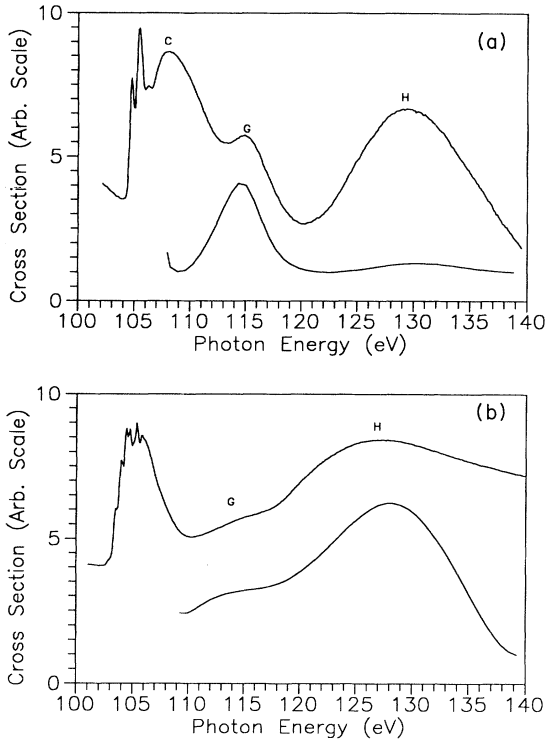

FIG. 5. (a) The Si $2p$ continuum spectra of $Si(OCH_3)_4$ (top) and the corresponding MS-$X\alpha$ SCF simulation (bottom). (b) The Si $2p$ continuum spectra of $Si(CH_3)_4$ (top) and the corresponding MS-$X\alpha$ SCF simulation (bottom).

above discrepancies notwithstanding, spectra of this similarity can only arise from almost identical electronic transitions in the two compounds and this is strong evidence that the Si $2p$ XANES features are dependent almost entirely upon the local environment of the central Si atom, with extended long-range structure playing only a minor role. A similar conclusion has been reached[28] for the Si $L_{2,3}$ edge in the spectra of the nesosilicates Mg_2SiO_2, Fe_2SiO_4, Be_2SiO_4, and Zn_2SiO_4.

Figures 4 and 5 show the preedge and continuum region of TMOS and TMS, respectively, together with their

TABLE III. The calculated orbitals, transition energies, term values, and oscillator strengths for the Si $2p$ edge of $Si(OCH_3)_4$ and $Si(CH_3)_4$. The corresponding experimental peak is shown in parentheses after the energy.

Orbital	Calc. Energy (expt. peak) $P_{3/2}$ (eV)	$P_{1/2}$ (eV)	Term value (eV)	Oscillator strength	Remark
$Si(OCH_3)_4$					
a_1^*	104.84(A)	105.45(A')	2.58	1.26×10^{-3}	Antibonding
a_1	105.68(B)	106.29(B')	1.74	2.67×10^{-4}	Mixed Ryd.
a_1^*	107.70(C)	108.31(C)	−0.28	9.24×10^{-4}	Antibonding
b_1^*	108.00(C)	108.61(C)	−0.58	3.61×10^{-4}	Antibonding
b_2^*	108.00(C)	108.61(C)	−0.58	3.61×10^{-4}	Antibonding
$Si(CH_3)_4$					
$4t_2^*$	103.67(B)	104.28(B')	2.19	1.55×10^{-3}	Rydberg p
$5t_2^*$	104.63(C)	105.24(C')	1.23	1.75×10^{-3}	Rydberg p
$2e^*$	104.90(D)	105.51(D')	0.96	1.11×10^{-4}	Rydberg d
$6t_2^*$	105.07(E)	105.68(E')	0.79	1.31×10^{-3}	Rydberg d
$7t_2^*$	105.29(F)	105.90(F')	0.57	3.45×10^{-4}	Rydberg p
$9t_2^*$	105.59(F')	106.20(F')	0.27	6.82×10^{-4}	Rydberg d
10_2^*	105.70	106.31	0.16	8.43×10^{-5}	Rydberg p
$13t_2^*$	105.85	106.46	0.01	3.87×10^{-4}	Rydberg d

respective MS-$X\alpha$ simulations. The simulation of TMS was carried out in T_d symmetry while that of TMOS was done in C_{2v} because the true S_4 symmetry of TMOS is not amenable to the MS-$X\alpha$ technique. The present results for the Si $2p$ edge of the TMS agree quantitatively with those of Bozek[23] and the assignments and oscillator strengths for TMOS and TMS are presented in Table III.

The simulated preedge spectra in Fig. 4 were calculated using the positions of the unoccupied molecular orbitals and their corresponding oscillator strengths. Each peak was coupled to its spin-orbit counterpart with a splitting of 0.613 eV and an intensity ratio of 2:1. Each transition was represented by a peak with a half-height width of 0.5 eV for TMOS and 0.4 eV for TMS and a 100% Lorentzian line shape. In both cases the simulated spectra had to be shifted by ~ 0.7 eV to align them with the experimental data.

The spectrum of TMS has already been described by Bozek, Bancroft, and Tan[23] and thus will not be discussed here in detail. The peaks in this spectrum result from transitions to Rydberg-type orbitals mostly of atomic p and d character.

The agreement between experiment and theory in TMOS is very good with all of the features in the experimental spectrum being represented in the simulation with the relative peak positions agreeing to within 0.2 eV. In C_{2v} symmetry the p orbitals have a_1, b_1, and b_2 symmetry for the p_z, p_x, and p_y orbitals, respectively. Wherever transitions from more than one p orbital occur at the same position (i.e., p_x+p_y, $p_x+p_y+p_z$, etc.), only the sum of the transitions is shown; that is, no distinction is made between a transition from a p_x, p_y, or p_z orbital.

The initial doublet, peaks A and A' in the simulation, results from a transition to an antibonding orbital of a_1^* symmetry which is split into a $p_{3/2}$ (peak A) and a $p_{1/2}$ (peak A') component. The reversal of the relative intensities of the spin-orbit doublet in experimental spectra is not uncommon in photoabsorption spectroscopy[23,24] and this phenomenon has been discussed by Schwarz.[29,30] It is important to note here that the relative intensities in the simulation agree very well with the solid-state spectrum of SiO_2 in Fig. 3(a).

Peak B', at 106.29 eV, is the $p_{1/2}$ component of a transition to a mixed Rydberg orbital of a_1 symmetry. If this peak in the simulation was given sufficient intensity to match its corresponding position in the experimental data, and its $p_{3/2}$ component (which is directly under peak A') was increased accordingly, then this would boost the intensity of peak A' in the simulation by a sufficient amount so as to match that of the experimental data. As noted in the discussion of the solid-state spectrum, the fact that peak B' does not appear at all in the spectrum of SiO_2, and the fact that the intensities of the initial doublet are reversed between the gas and solid state, suggest that the transition which is responsible for peak B' in TMOS is not present in SiO_2. This issue is addressed below.

The broadband at ~ 108 eV (peak C) results from three transitions to three unoccupied orbitals of a_1^*, b_1^*, and b_2^* symmetry, all three of which are just above the ionization threshold. The b_1^* and b_2^* orbitals are isoenergetic and thus show up as only a single spin-orbit doublet, the other doublet arising from the transition to the a_1^* orbital. (In T_d symmetry these three orbitals combine to form the t_2^* antibonding orbital as will be discussed in reference to Fig. 6.) The broad nature of this peak in the experimental data suggests that there may be several other transitions here, such as Rydberg states, that are not accounted for in the simulation. This may be a manifestation of the fact that the simulation was carried out in C_{2v} symmetry while the true symmetry of the molecule is actually S_4.

The continuum region shown in Fig. 5 is represented reasonably well by the calculations for TMOS and very well for TMS. Peak G in both spectra result from a d-shape resonance[31] of e symmetry and is simulated very well by the $X\alpha$ calculation. The second peak, H (at ~ 130 eV), which should be very intense, shows up only as a very weak peak in the simulation of TMOS. This peak is present in virtually every Si $2p$ photoabsorption spectrum of all Si-containing compounds. Its position at ~ 130 eV is coincident with the maximum of the Si $2p$ cross section and this, coupled with its ubiquitous presence in all Si $2p$ spectra, strongly suggests that it is the result of an atomic effect that is largely independent of the ligands to which the Si is attached. The fact that this is likely an atomic effect and thus independent of the orbital structure of TMOS may account for the poor correspondence between theory and experiment in this region of the Si $2p$ spectrum of TMOS. Peak D has also been assigned (in the Si L-edge spectra of other Si compounds[31]) to the t_2 component of a d-shape resonance. Although not a perfect match, the $X\alpha$ simulation of TMOS is a better theoretical model for the Si $2p$ spectrum of SiO_2 than the DOS calculation[26] [see Fig. 3(a)] and has the distinct advantage of being more economical in terms of both time and cost. Only minor peaks—peak B' in TMOS (Fig. 2) and D in SiO_2 [Fig. 3(a)]—are not common to both spectra.

Derived from the MS-$X\alpha$ calculations, Fig. 6 shows a molecular-orbital (MO) diagram for TMOS in C_{2v} symmetry and the corresponding orbitals in tetrahedral symmetry. For the sake of simplicity, the only orbitals shown are the occupied orbitals that constitute Si-O bonds and the first four unoccupied orbitals; namely, the first two a_1^* orbitals, the first b_1^*, and the first b_2^* orbital. The orbitals in T_d symmetry were composed from those in C_{2v} from a standard group theory correlation table. To the left of each orbital in T_d symmetry is the combination of irreducible representations in C_{2v} from which it is composed and to the right is the T_d irreducible representation to which it belongs. The ordering of the orbitals in T_d is identical to that of similar MO diagrams[10,11] calculated for SiO_4^{4-} except that the ordering of the first two unoccupied states in the present calculation is reversed compared to that of Tossell.[10] This reversal is consistent with more recent calculations by McComb *et al.*[32] The positions of the occupied states in this calculation and those of Tossell[10] are compared in Table IV along with the positions of peaks in the valence-band photoelectron spectra of TMOS and SiO_2.

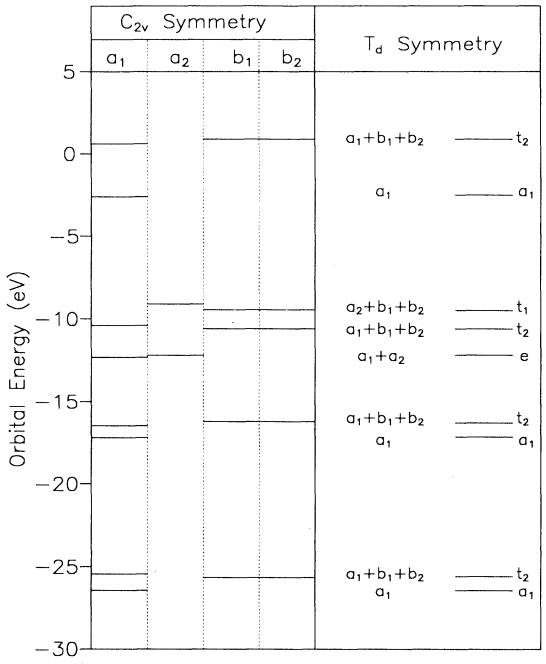

FIG. 6. Molecular-orbital diagram for $Si(OCH_3)_4$ in C_{2v} and T_d symmetries. To the left of the orbitals in T_d symmetry is the combination of C_{2v} irreducible representations from which they are comprised and to the right is the T_d representation to which they belong.

The absolute values of the molecular-orbital energies calculated for TMOS and SiO_4^{4-} are quite different mainly because of the large negative charge on the latter species, but the ordering is the same and the relative differences between states are very close in the two analogs.

From Table III and the MO diagram in Fig. 6 it can be seen that the first three peaks in the Si $2p$ spectrum of TMOS (Peaks A, A', and B' in Fig. 2) result from transitions to two orbitals of a_1 symmetry, the first being antibonding and the second being mixed Rydberg in character. The second of these orbitals (the mixed Rydberg orbital) has been omitted from the MO diagram in Fig. 6 because transitions to Rydberg-type orbitals are usually washed out in solid-state spectra. The next three orbitals in TMOS are an a_1^*, a b_1^*, and a b_2^*. These three orbitals are approximately isoenergetic and combine to form the t_2^* in tetrahedral symmetry. With this in mind it is reasonable to suggest that the initial doublet in the spectrum of SiO_2 results from a transition to a molecular orbital of a_1^* symmetry and that peak C in the spectrum of SiO_2 results from a transition to the t_2^* orbital. This type of assignment, based upon a molecular-orbital interpretation of SiO_2, is very similar to that proposed by Filatova, Vinogrdov, and Zimkina.[7]

Figure 7 shows a comparison of the photoelectron spectra of TMOS and SiO_2. The data for the valence-band photoelectron spectrum of SiO_2 have been digitized from DiStefano and Eastman,[2] deconvoluted with a series of 100% Gaussian peaks, and shifted by 7 eV to better align it with the gas-phase spectrum. This spectrum has been interpreted by Tossell[10] in a fashion similar to that used for SiF_4 with the three lowest energy bands assigned to nonbonding orbitals of t_1, t_2, and e symmetry. Although this assignment is correct for SiF_4 or SiO_4^{4-}, it is not strictly correct for either SiO_2 or $Si(OCH_3)_4$. In the latter two cases each oxygen atom forms two bonds—to a second Si in SiO_2 or to a C in $Si(OCH_3)_4$—and thus there are not enough nonbonding

TABLE IV. The positions of the Si-O bonding orbitals from the photoelectron spectra of $Si(OCH_3)_4$ and SiO_2 (Fig. 7), the calculated positions of the MO's of $Si(OCH_3)_4$ (Fig. 6), and the calculated MO's for SiO_4 (Ref. 10). Both experimental and calculated values for SiO_2 have been shifted by 7 eV for comparison with the gas-phase data. The positions of the C-O and C-H bonding orbitals in $Si(OCH_3)_4$ (Fig. 7) are also listed.

Peak assignment	$Si(OCH_3)_4$ (eV)	SiO_2 (+ 7 eV)	SCF Calc. (eV)	SCF Calc. (Ref. 10) (− 7 eV)
t_1	8.95	8.05	−9.48	−7.0
t_2	9.71	9.37	−10.60	−8.0
e	10.71	10.97	−12.17	−8.5
C-O	13.22			
t_2	13.99	13.63	−16.22	−12.4
C-H	13.99			
a_1	16.71	16.80	−17.5	−15.5

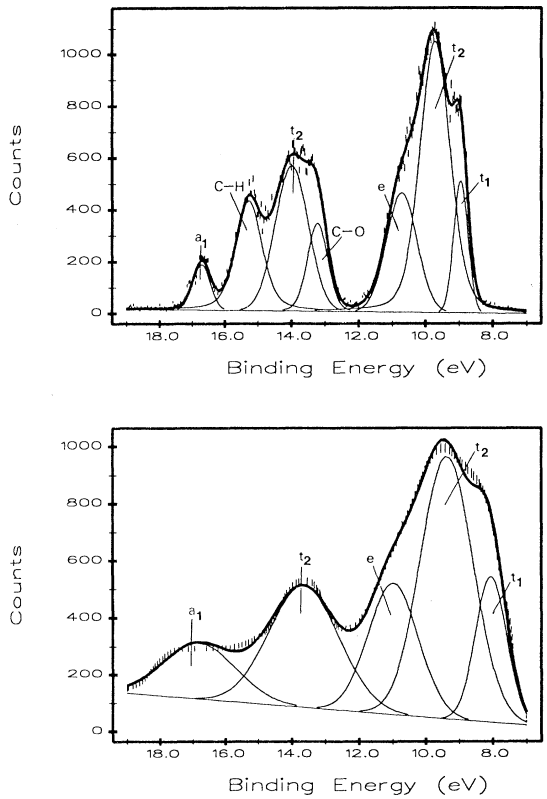

FIG. 7. (a) The gas-phase valence-band photoelectron spectra of $Si(OCH_3)_4$ and (b), the valence band of solid-state SiO_2. (b) is digitized from Ref. 2 and the energies have been shifted by 7 eV to better align with the gas-phase data.

electrons on the four oxygen atoms to fill the three nonbonding orbitals. Despite this problem in SiO_2 and $Si(OCH_3)_4$, the Tossell-type assignment is in excellent qualitative agreement with band-structure calculations[33,34] on SiO_2 and hence Tossell's MO assignment has been repeated here for the sake of comparison.

Although qualitatively very similar, the two spectra of TMOS and SiO_2 show that the occupied states in SiO_2 are separated from each other slightly more than they are in TMOS but it is impossible to say whether or not this trend also applies to the unoccupied antibonding orbitals. The largest peak, at ~10 eV in both Figs. 7(a) and 7(b), corresponds to ionizations of the three nonbonding orbitals of t_1, t_2, and e symmetry in Fig. 6. The second largest peak in both spectra is centered at ~14 eV. In SiO_2 this corresponds to the Si-O bonding orbital of t_2 symmetry while in TMOS there are three components: (1) the O-C bonding orbital at 13.22 eV, (2) the Si-O bonding orbital at 13.99 eV (t_2 in Fig. 6), and (3) the C-H bonding orbitals at ~15.27 eV. The final peak at ~17 eV corresponds to the Si-O bonding orbitals of a_1 symmetry in SiO_2 and TMOS. The excellent agreement between the valence-band photoelectron spectra of TMOS and SiO_2 is further testimony to the similarity of the electronic structure in these two systems.

The Si 1*s* and 2*s* edges

Figure 8 shows the Si 1*s* photoabsorption spectra of the five compounds in the series $Si(CH_3)_x(OCH_3)_{4-x}$ from 1830 to 1880 eV and Table V gives the positions of the peaks. The spectra of TMOS and TMS have been reported before and although the current work agrees well with previously reported spectra of TMS,[15,16] the previously reported spectrum of TMOS (Ref. 16) shows only a single broad peak where Fig. 8 shows beyond any doubt that this actually consists of at least two peaks. This fact is further supported by inspection of the spectra of the intermediate compounds in which this second peak is seen to increase in stoichiometric proportion to the number of methoxy groups in the molecule. The spectra of TMOS and TMS are qualitatively similar to those of SiF_4 and $SiCl_4$ in which the spectra consist of one (or two in the case of SiF_4) sharp transition followed by two or three relatively weak peaks at higher energy.[15]

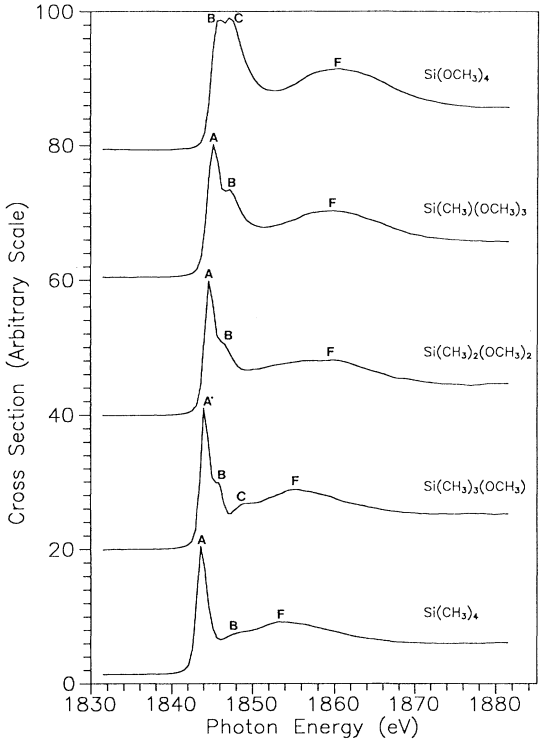

FIG. 8. The Si 1*s* XANES spectra of the five compounds in the series $Si(CH_3)_x(OCH_3)_{4-x}$ ($x = 0$ to 4).

Figure 9(a) shows the spectra of the 1*s* regions in TMOS and SiO_2 and the DOS calculation (shifted by 1835 eV) all plotted on the same axes and Fig. 9(b) shows the comparison of the Si 1*s* spectrum of TMS and silicon carbide (digitized from Ref. 35). The main peak in the spectrum of SiC is extremely broad and likely consists of several different transitions while the corresponding peak in SiO_2 is very narrow—narrower even than the corresponding peak in TMS. Furthermore, the spectrum of SiO_2 shows only a single sharp peak whereas the gas-phase analog, TMOS, has an obvious doublet structure.

TABLE V. The positions (in eV) of the peaks in the spectra shown in Figs. 8 and 9(a), and the Si 1*s* binding energies. The binding energies of $Si(OCH_3)_4$ and $Si(CH_3)_4$ were determined by comparison of the term values with those of the *L*-edge spectra and the binding energies of the three intermediate compounds were approximated by linear interpolation from the two end members of the series.

	Molecule $Si(OCH_3)_x(CH_3)_{4-x}$			(Fig. 8)		(Fig. 9)	
Peak	$x=0$	$x=1$	$x=2$	$x=3$	$x=4$	SiO_2	DOS (+ 1835 eV)
A	1843.6	1844.0	1844.6	1845.2			
B	1848.5	1845.6	1846.5	1847.2	1845.9	1845.1	1845.1
C		1849.1			1847.3	1846.8	1846.8
D						1850.9	1850.5
E						1854.5	1855.4
F	1853.3	1855.3	1859.7	1859.8	1860.6	1857.3	1856.9
Si 1*s*	1845.8	1846.3	1846.7	1847.2	1847.6		

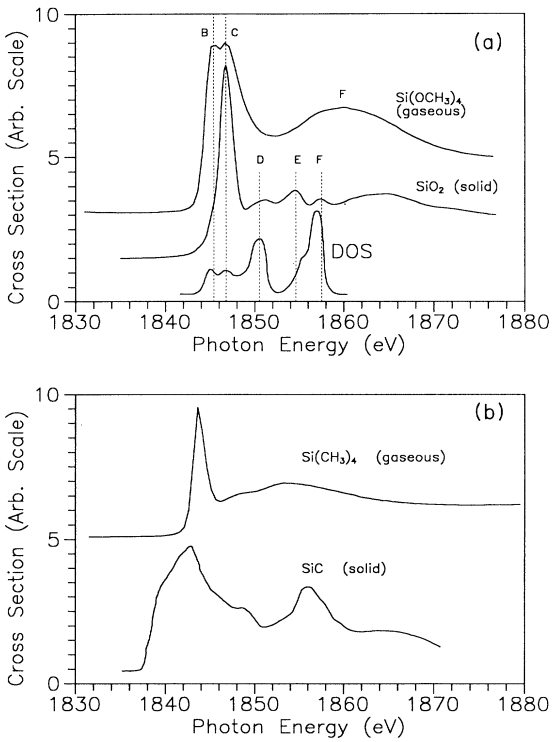

FIG. 9. (a) Comparison of the Si 1s XANES spectra of gas-phase $Si(OCH_3)_4$ and solid-state SiO_2. (b) Comparison of the Si 1s XANES spectra of gas-phase $Si(CH_3)_4$ and solid-state SiC.

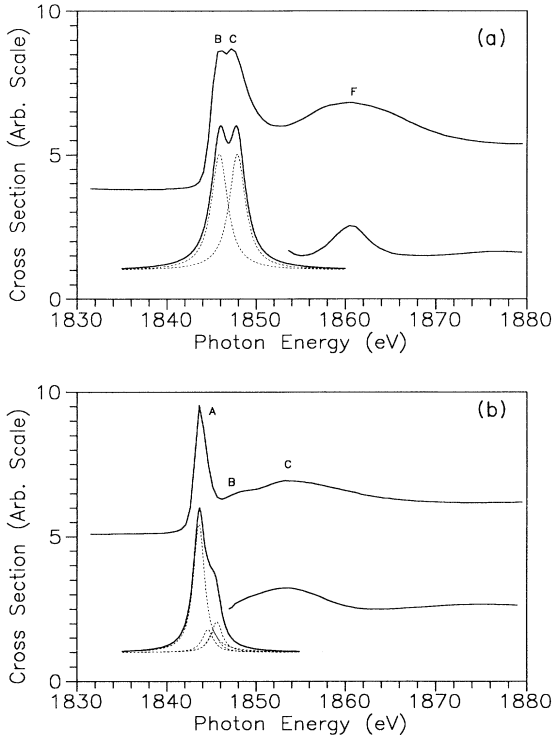

FIG. 10. (a) The Si 1s XANES spectra of $Si(OCH_3)_4$ (top) and the corresponding MS-$X\alpha$ SCF simulation (bottom). (b) The Si 1s XANES spectra of $Si(CH_3)_4$ (top) and the corresponding MS-$X\alpha$ SCF simulation (bottom). Dashed lines in both (a) and (b) mark the positions of the individual transitions.

The absence of this doublet in the solid-state spectrum is discussed below in the analysis of the MS-$X\alpha$ simulation.

Not only are the preedge features dissimilar, but the continuum shows, perhaps, an even more pronounced difference; however, the continuum features in the solid state do show a qualitative correspondence to the DOS calculation. The fact that there seems to be little correspondence between the gas phase and the solid-state spectra in both the preedge and the continuum regions of the 1s edge implies that, unlike the Si 2p spectra, the extended long-range structure of the solid-state SiO_2 has a significant effect on the K-edge spectra.

Figure 10 shows the 1s region of TMOS and TMS together with their respective simulations of the preedge and the continuum shown below the experimental data and Fig. 11 shows the same plot of the 2s region. Table VI lists the peak positions, term values, assignments, and oscillator strengths for both the 1s and 2s regions of TMOS and TMS. Because the 2s peak is so weak (see Fig. 1) no continuum calculation was performed in this study. Although the overall shape of the simulations matches that of the experimental data very well, the calculated oscillator strengths are much too low for the Si K edge of both TMOS and TMS. This results from a large integration mesh that leads to numerical instability when calculating the overlap integral between a very contracted 1s and an oscillating outgoing wave. However, because the 1s region is so similar to the 2s (which is less contracted and hence unaffected by a large integration mesh), and because of the close match between the theory and the experimental data, it is felt that the poor reproduction of the 1s oscillator strength is (comparatively) unimportant to this paper.

In TMOS the experimental and simulated data match very well in terms of peak position in the 1s region but the simulation of the 1s continuum is much too narrow. The preedge features consist of two transitions, both to bound states of a_1 symmetry, with half-height linewidths of 2.0 eV. The 2s region of TMOS is essentially identical, but had to be deconvoluted with a slightly broader linewidth (2.5 eV) to create one contiguous peak as seen in the experimental data. The term values of the two peaks in both the Si 1s and 2s regions are very close with values of 1.70 and -0.23 eV for the two peaks in the 1s spectrum and 1.76 and -0.25 eV for the same two peaks in the 2s spectrum (see Table VI). These values are essentially the same as the second and third transitions in the Si 2p spectrum (Table III) which have term values of 1.74 and -0.28 eV, respectively.

As mentioned above, peaks B and C in the 1s spectrum of TMOS result from transitions from the 1s orbital to two different orbitals of a_1 symmetry. Both of these transitions are allowed in C_{2v}. In tetrahedral symmetry only transitions from the 1s to orbitals of t_2 symmetry are allowed. The second a_1^* orbital (peak C) in tetrahedral symmetry is the a_1 component of the t_2^* orbital, and thus

this transition is allowed in SiO_2. The first a_1^* orbital (peak *B*) does not transform as the t_2 in tetrahedral symmetry and thus this transition should be completely forbidden in the *K*-edge spectrum of SiO_2 (Fig. 9). The weak shoulder on the low-energy side of peak *C* in SiO_2 does, however, line up with peak *B* in the spectrum of TMOS, suggesting that this transition is weakly allowed even in the tetrahedral environment of SiO_2.

The experimental linewidths of the 1*s* and 2*s* regions are nearly identical in the case of both TMOS and TMS; however, in the former molecule the 2*s* peak is slightly broader, which obscures the separation of the two peaks. Otherwise, although the relative oscillator strengths differ, the term values for the 1*s* and 2*s* regions are essentially identical (see Table VI). Because of the strong background in the 2*s* region of TMOS, direct comparison of the 1*s* and 2*s* regions in this compound is difficult. However, it is interesting to note that the 1*s* and 2*s* regions in TMS are essentially identical, both consisting of a sharp peak with a half-height width of 1.65 eV followed by two weak features in the continuum which occur at 3.9 and 9.5 eV above the main peak [these are peaks *A*, *B*, and *C* in Figs. 10(b) and 11(b)]. Furthermore, comparison of the 1*s* region in Fig. 8 with the 2*s* region in Fig. 1 shows remarkable similarities indicating that the features in these regions result from transitions to the same unoccupied orbitals as indicated by the essentially equivalent term values documented in Table VI.

In TMS both the 1*s* and 2*s* regions are dominated by a single strong transition to a bound orbital of t_2 symmetry accompanied by three smaller transitions each with a linewidth of 1.5 eV. The shoulder on the high-energy

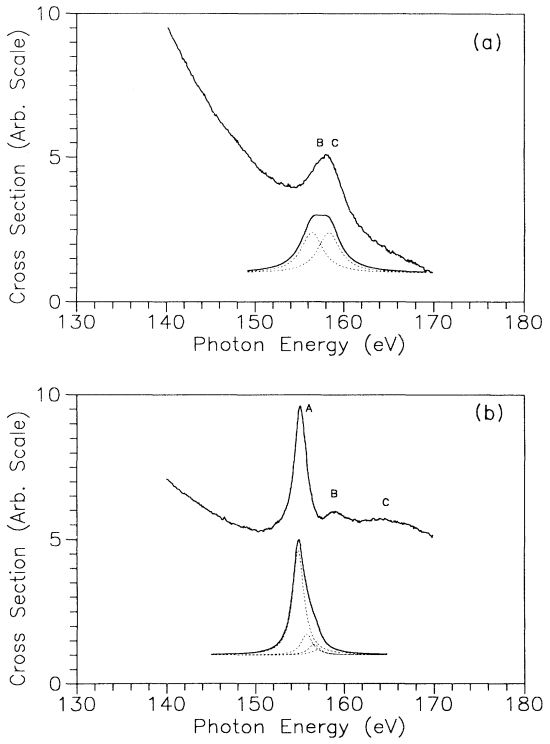

FIG. 11. (a) The Si 2*s* XANES spectra of $Si(OCH_3)_4$ (top) and the corresponding MS-$X\alpha$ SCF simulation (bottom). (b) The Si 2*s* XANES spectra of $Si(CH_3)_4$ (top) and the corresponding MS-$X\alpha$ SCF simulation (bottom). Dashed lines in both (a) and (b) mark the positions of the individual transitions.

TABLE VI. The calculated orbitals, transition energies, term values, and oscillator strengths for the Si 1*s* and Si 2*s* edges of $Si(OCH_3)_4$ and $Si(CH_3)_4$. The corresponding experimental peak is shown in parentheses after the energy.

Orbital	Energy (expt. peak) (eV)	Term value (eV)	Oscillator strength	Remark
$Si(OCH_3)_4$ 1*s*				
a_1	1845.90 (*B*)	1.70	1.37×10^{-8}	Mixed Ryd.
a_1^*	1847.83 (*C*)	−0.23	1.42×10^{-8}	Antibonding
$Si(OCH_3)_4$ 2*s*				
a_1	156.26 (*B*)	1.76	2.67×10^{-5}	Mixed Ryd.
a_1^*	158.12 (*C*)	−0.25	2.61×10^{-5}	Antibonding
$Si(CH_3)_4$ 1*s*				
$4t_2^*$	1843.65 (*A*)	2.18	9.95×10^{-9}	Rydberg *p*
$5t_2^*$	1844.62 (*A*)	1.21	1.78×10^{-9}	Rydberg *p*
$7t_2^*$	1845.26 (*A*)	0.57	1.58×10^{-9}	Rydberg *p*
$10t_2^*$	1845.69 (*A*)	0.14	2.39×10^{-9}	Rydberg *p*
$Si(CH_3)_4$ 2*s*				
$4t_2^*$	154.64 (*A*)	2.20	4.97×10^{-5}	Rydberg *p*
$5t_2^*$	155.67 (*A*)	1.23	1.00×10^{-5}	Rydberg *p*
$7t_2^*$	156.25 (*A*)	0.59	5.01×10^{-6}	Rydberg *p*
$10t_2^*$	156.71 (*A*)	0.13	2.43×10^{-6}	Rydberg *p*

side of the 1s simulation seems to have no counterpart in the experimental data. The 2s region of TMS is represented by exactly the same four transitions but the slight difference in relative oscillator strengths in the 2s region yields a better agreement with the experimental data.

The cross section in the Si 1s region (preedge and continuum) is much smaller than that of the corresponding 2p region. Above-edge features in the 2p spectra are dominated by intense shape resonances that swamp any small peaks that may be due to the extended band structure or multiple scattering. In the 1s region, because the cross section is much lower, small peaks due to multiple scattering of the outgoing electron wave become apparent. Because the scattering process depends on long-range structure (at least three atoms from the central species), only very large gas-phase molecules such as $Si[Si(CH_3)_3]_4$ and $Ge[Si(CH_3)_3]_4$ will be helpful in the analysis of K-edge solid-state spectra.[36] However, because multiple scattering plays only a very minor role in the L-edge spectra, gas-phase compounds may be used here as excellent models for solid-state systems.

THE L EDGE OF THE OXIDES OF THE THIRD-ROW ELEMENTS

Having established that the L-edge spectra of the gas-phase TMOS and solid-state SiO_2 are very similar, it is interesting to compare the L-edge spectra of analogous tetrahedral oxides of the third-row elements. Figure 12 shows the spectrum of SiO_2, $(Ca)_3(PO_4)_2$, Na_2SO_4, and $NaClO_4$ all plotted on the same scale and Table VII documents the pertinent data. In each compound, the zero point marks the position of the ionization edge.[37] Certain similarities are readily apparent between the four spectra and each spectrum can be broken down into three main regions relative to their respective ionization thresholds: (i) 0–8 eV, (ii) 8–15 eV, and (iii) 15 eV and above.

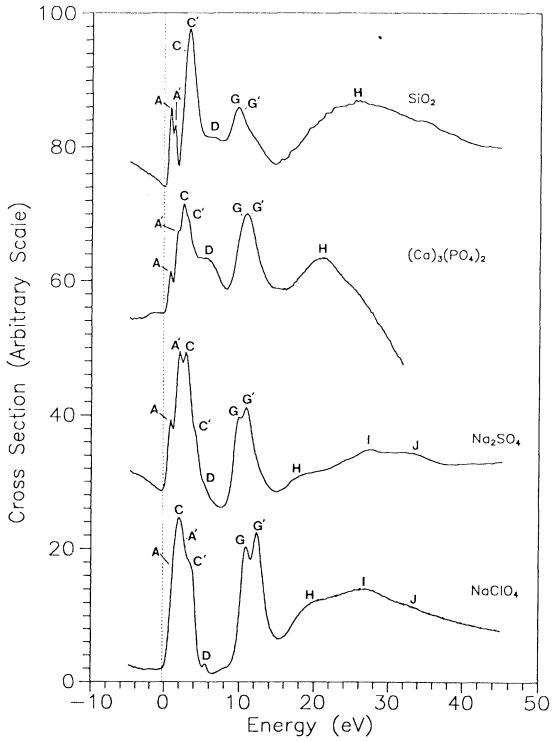

FIG. 12. The 2p XANES spectra of the four isoelectronic species SiO_2, PO_4, SO_4, and ClO_4 shifted by 103.65, 131.10, 169.40, and 208.70 eV, respectively, so that the 2p ionization energy has a value of 0.00 eV. The 2p ionization energies were taken from Ref. 37.

As one moves across the third row of the Periodic Table, the peaks in the first region of Fig. 12 seem to broaden out and coalesce into one broad peak. Part of this broadening is due to the steady increase in the spin-orbit splitting: 0.613 for Si,[23,25] 0.86 for P,[38] 1.21 for S,[38] and 1.64 for Cl.[39] A second reason for the broadening and coalescence is the decrease in the lifetime of the 2p hole as one moves across the period, although this is likely a negligible effect because the linewidths here are so much broader than the lifetime widths which are all less than 0.15 eV.

From an analysis of the valence-band photoelectron spectra[40] and of molecular-orbital calculations[41] of the three isoelectronic anions, PO_4^{3-}, SO_4^{2-}, and ClO_4^-, it is obvious that the occupied MO's span a greater range of energy as one moves across the period from phosphorus to sulfur to chlorine. However, the same MO calculations[41] show that the exact opposite is true in the case of the unoccupied antibonding orbitals. That is, the antibonding orbitals become more compressed and span a lesser range of energies as this period is traversed from P to Cl.

It then stands to reason that if the first peaks in the Si 2p spectrum of SiO_2 (A, A', C, and C' in Fig. 12) result from transitions to a_1^* and t_2^* orbitals, then the first peaks in the spectra of the isoelectronic anions, PO_4^{3-}, SO_4^{2-}, and ClO_4^-, should also result from the same transitions. Furthermore, because the energies of the unoccupied orbitals become compressed[41] as one moves from P to Cl, one would expect these peaks to coalesce due to the fact that the a_1^* and t_2^* become closer together. The compression of the unoccupied orbitals coupled with the increase in spin-orbit splitting explains the trend in the first region of these spectra. In all four spectra, peaks A and A' result from the $p_{3/2}$ and $p_{1/2}$ components of a transition to an a_1^* antibonding orbital and peaks C and C' are the

TABLE VII. The peak positions (in eV) relative to their 2p ionization edges and assignments for the four spectra shown in Fig. 12.

Peak	SiO_2	PO_4	SO_4	ClO_4	Assignment
A	0.73	0.82	0.79	1.20	$p_{3/2}\rightarrow a_1^*$
A'	1.30	1.76	2.06	2.78	$p_{1/2}\rightarrow a_1^*$
C	2.93	2.43	2.73	2.01	$p_{3/2}\rightarrow t_2^*$
C'	3.49	3.33	4.04	3.62	$p_{1/2}\rightarrow t_2^*$
D	6.72	5.51	5.28	5.54	Multiple scattering
G	9.64	10.11	9.80	10.80	$p_{3/2}\rightarrow d$-shape res.
G'	10.25	11.00	11.04	12.35	$p_{1/2}\rightarrow d$-shape res.
H	25.7	20.8	18.6	20.5	Maximum of atomic cross section
I			27.3	26.5	Multiple scattering
J			32.9	33.1	Multiple scattering

$p_{3/2}$ and $p_{1/2}$ components of a transition to a t_2^* antibonding orbital. In the case of ClO_4^-, the a_1^* and t_2^* are so close together that the $p_{3/2}$ peak of the t_2^* (peak C) is at a lower energy than the $p_{1/2}$ peak of the A_1^* (peak A'). Peak D in this same region also shifts closer to the ionization edge as the period is traversed from Si to Cl; however, the low intensity and large linewidth has prevented resolution of the spin-orbit splitting on this feature.

The second region, from 8 to 15 eV, has a very strong absorption band in each spectrum (peaks G and G'). In SiO_2 this peak is quite broad, becoming sharper in PO_4^{3-} and then splitting in the case of SO_4^{2-} and splitting even more so in the case of ClO_4^-. The splitting of this peak in the latter two species results from their respective spin-orbit splitting of 1.21 eV for S and 1.64 eV for Cl. The shoulder on the high-energy side of this peak in the spectrum of SiO_2 is coincident with a large peak in the DOS calculation presented in Fig. 3(a). The $X\alpha$ simulations of TMOS suggest that peak G is due to a d-shape resonance in TMOS and SiO_2 and thus a similar assignment has been made for the other three solid-state spectra in Fig. 12.

The third region consists of a single broad structureless peak in the case of SiO_2 and PO_4^{3-} with the last two compounds showing more structure in this area. In all four cases peak H corresponds to the position of the cross-section maximum[42] for the $2p$ level of Si, P, S, and Cl relative to their respective $2p$ ionization edges. Peak H has also been attributed to a t_2 shape resonance and this may also account for some of the intensity. Peaks I and J for the S and Cl moieties may be due to multiple scattering of the outgoing electron. Other differences in these four spectra may be due to manifestations of the different counter ions in the four examples shown.

CONCLUSIONS

The $Si(OCH_3)_4$ molecule (TMOS) is an excellent experimental model for the Si $2p$ photoabsorption spectrum and the valence-band photoelectron spectrum of SiO_2. The features in the Si $2p$ XANES spectrum of SiO_2 are due primarily to the local structure surrounding the Si atom with long-range order playing only a minor role. Furthermore, the MS-$X\alpha$ SCF calculations on TMOS provide, perhaps, the best explanation of the Si $2p$ spectrum of SiO_2 to date. Density-of-states calculations may be helpful in this regard but are considerably more time consuming as well as being more expensive, and calculations done on the SiO_4^{4-} ion suffer from the effects of having a single dangling bond on each of the oxygens.

Gas-phase molecules can be used to model the spectra of solid-state compounds in the low-energy domain where cross sections are high. For K-edge spectra, or wherever the cross section is low, the dominant features in the above edge region of the XANES spectra of solids will be the result of the extended long-range structure (as reflected in the DOS calculations) or due to multiple scattering of the electron wave off of neighboring atoms in the matrix.

The L-edge spectra of the four isoelectronic species SiO_4^{4-}, PO_4^{3-}, SO_4^{2-}, and ClO_4^- are qualitatively very similar despite the fact that their respective $2p$ ionization thresholds range from 103.6 eV for SiO_2 to 208.7 eV for ClO_4^-. This is further evidence that the solid-state spectra can be interpreted in terms of molecular-orbital theory derived from small molecular analogs.

A suggested use of gas-phase systems to interpret solid-state phenomena is in the case of the interfacial regions between bulk Si and SiO_2 monolayers where the actual oxidation state of Si is in question. Here a series of molecules such as $Si[Si(CH_3)_3]_x[OCH_3]_{4-x}$ could be synthesized which mimic the effect of one to four oxygens bonded to a silicon atom in the bulk Si environment. This type of work has already been done by Sutherland, Bancroft, and Tan in which the series $Si[Si(CH_3)_3]_xH_{4-x}$ was successfully used to mimic the effect of one to four hydrogens bonded to a silicon atom on a Si surface.[25]

*Author to whom correspondence should be addressed.

[1]J. L. Dehmer, J. Chem. Phys. **56**, 4496 (1971).
[2]T. H. DiStefano and D. E. Eastman, Phys. Rev. Lett. **27**, 1560 (1971).
[3]F. C. Brown, R. Z. Bachrach, and M. Skibowski, Phys. Rev. B **15**, 4781 (1977).
[4]A. Bianconi, Surf. Sci. **89**, 41 (1979).
[5]A. Bianconi and R. S. Bauer, Surf. Sci. **99**, 76 (1980).
[6]G. Hollinger and F. J. Himpsel, Appl. Phys. Lett. **44**, 93 (1983).
[7]E. O. Filatova, A. S. Vinogrdov, and T. M. Zimkina, Fiz. Tverd. Tela (Leningrad) **27**, 997 (1985) [Sov. Phys. Solid State **27**, 606 (1985)].
[8]F. J. Himpsel, F. R. McFeely, A. Taleb-Ibrahimi, and J. A. Yarmoff, Phys. Rev. B **38**, 6084 (1988).
[9]G. R. Harp, Z. L. Han, and B. P. Tonner, J. Vac. Sci. Technol. A **8**, 2566 (1990).
[10]J. A. Tossell, J. Am. Chem. Soc. **97**, 4840 (1975).
[11]J. A. Tossell, D. J. Vaughan, and K. H. Johnson, Chem. Phys. Lett. **20**, 329 (1973).
[12]K. H. Tan, G. M. Bancroft, L. L. Coatsworth, and B. W. Yates, Can. J. Phys. **60**, 131 (1982).
[13]R. Haensel, C. Keitel, P. Schreiber, and C. Kunz, Phys. Rev. **188**, 1375 (1969).
[14]B. X. Yang, F. H. Middleton, B. G. Olson, G. M. Bancroft, J. M. Chen, T. K. Sham, K. Tan, and D. J. Wallace, Nucl. Instrum. Methods Phys. Res. **316**, 422 (1992).
[15]S. Bodeur, P. Millie, and I. Nenner, Phys. Rev. A **34**, 2986 (1986).
[16]S. Bodeur, P. Millie, and I. Nenner, Phys. Rev. A **41**, 252 (1990).
[17]J. D. Bozek, J. N. Cutler, G. M. Bancroft, L. L. Coatsworth, K. H. Tan, D. S. Yang, and R. G. Cavell, Chem. Phys. Lett. **165**, 1 (1990).
[18]M. Kasrai, M. E. Fleet, T. K. Sham, G. M. Bancroft, K. H. Tan, and J. R. Brown, Solid State Commun. **68**, 507 (1988).
[19]K. H. Johnson, Adv. Chem. Phys. **7**, 143 (1973).
[20]J. W. Davenport, Ph.D. thesis, University Pennsylvania (1976).
[21]L. Latter, Phys. Rev. **99**, 510 (1955).
[22]*Numerial Data and Functional Relationships in Science and*

Technology, edited by K. W. Hellwege and A. M. Hellwege (Springer-Verlag, New York, 1976), Vol. 7, p. 296 and Vol. 15, p. 454.
[23]J. D. Bozek, G. M. Bancroft, and K. H. Tan, Chem. Phys. **145**, 131 (1990), and references therein.
[24]J. S. Tse, Z. F. Liu, J. D. Bozek, and G. M. Bancroft, Phys. Rev. A **34**, 2986 (1989).
[25]D. G. J. Sutherland, G. M. Bancroft, and K. H. Tan, J. Chem. Phys. **97**, 7918 (1992).
[26]R. N. Nucho and Anupam Madhukar, Phys. Rev. B **21**, 1576 (1980).
[27]D. Li, G. M. Bancroft, M. Kasrai, M. E. Fleet, X. E. Feng, K. H. Tan, and B. X. Yang (unpublished).
[28]D. W. McComb, P. L. Hansen, and R. Brydson, Microsc. Microanal. Microstruct. **2**, 561 (1991).
[29]W. H. E. Schwarz, Chem. Phys. **13**, 153 (1976).
[30]W. H. E. Schwarz, Chem. Phys. **11**, 217 (1975).
[31]Z. F. Liu, J. N. Cutler, G. M. Bancroft, K. H. Tan, R. G. Cavell, and J. S. Tse, Chem. Phys. **168**, 133 (1992).
[32]D. W. McComb, R. Brydson, P. L. Hansen, and R. S. Payne, J. Phys. Condens. Matter **4**, 8363 (1992).
[33]J. R. Chelikowsky and M. Schlüter, Phys. Rev. B **15**, 4020 (1977).
[34]Yong-nian Xu and W. Y. Ching, Phys. Rev. B **44**, 11 048 (1991).
[35]Ph. Sainctavit, J. Petiau, C. Laffon, A.-M. Flank, and P. Lagarde, *X-Ray Absorption Fine Structure,* edited by S. S. Hasnain (Ellis Harwood, New York, 1991), pp. 38–40.
[36]J. Li, D. G. J. Sutherland, T. K. Sham, G. M. Bancroft, and K. H. Tan (unpublished).
[37]*Practical Surface Analysis by Auger and X-ray Photoelectron Spectroscopy,* edited by D. Briggs and M. P. Seah (Wiley, New York, 1983).
[38]R. G. Cavell and K. H. Tan, Chem. Phys. Lett. **197**, 161 (1992).
[39]K. Ninomiya, E. Ishiguro, S. Iwata, A. Mikuni, and T. Sasaki, J. Phys. B **14**, 1777 (1981).
[40]V. I. Nefedov, YU. A. Buslaev, N. P. Sergushin, YU. V. Kokonuv, V. V. Kovalev, and L. Bayer, J. Electron. Spectrosc. Relat. Phenom. **6**, 221 (1975).
[41]H. Johansen, Theor. Chim. Acta **32**, 273 (1974).
[42]J. J. Yeh and I. Lindau, At. Data Nucl. Data Tables **32**, 1 (1985).